Contents lists available at SciVerse ScienceDirect

CIRP Annals Manufacturing Technology

Journal homepage: www.elsevier.com/locate/cirp

Surface texturing to enhance sol-gel coating performances for biomedical applications

Andrea Ghiotti[a] (2), Rachele Bertolini[a], Luca Pezzato[a], Enrico Savio[a] (1), Mara Terzini[b], Stefania Bruschi[a] (1)

[a]*Department of Industrial Engineering, University of Padova, Via Venezia 1, 35131, Padova, Italy*
[b]*Department of Mechanical and Aerospace Engineering, Politecnico di Torino, C.so Duca degli Abruzzi 24, 10129, Torino, Italy*

The paper proposes a novel approach to increase the performances of a sol-gel coating for biomedical applications. In particular, ultrasonic vibration-assisted turning in combination with cryogenic cooling is explored for the first time to generate a complex and isotropic texture more prone to be coated, and, in turn, less corrosion susceptible compared to the corresponding surfaces generated through conventional machining. A comprehensive characterization of the generated surfaces before and after coating gives new insights for understanding the mechanisms of increased performances, which were validated on bones fixation pins.

Vibration, Texture, Magnesium

1. Introduction

Bioresorbable metals, as are magnesium alloys, are becoming more and more attractive for manufacturing temporary devices to fix bone fractures [1] since, apart from obviating secondary operations for their removal, they also reduce the occurrence of artefacts during postoperative imaging. A key functionality to be controlled in their manufacturing is assuring a well-paced degradation inside the human body while the bone is healing, specifically by increasing the corrosion resistance of the temporary device.

Coating of the bioresorbable metal substrate may represent a suitable way to increase corrosion protection; nevertheless, performances of coatings strongly depend on their thickness [2], homogeneity, and adhesion strength with the substrate. To improve coating adhesion, structured surfaces have been proved effective to control the wetting state of a surface [3]. Texture modification is indeed more and more widespread for metal surfaces functionalization for a wide range of applications, including those in the biomedical field. The manufacture of specific surface textures for increasing functional performances can be fulfilled through different methods. Laser-based processes are interesting thanks to their high flexibility in generating textures of high complexity and accuracy [4]. Unfortunately, surface and sub-surface damaging associated to laser texturing can substantially alter the surface integrity impairing the requested performances. On the other hand, cutting processes have the potential to avoid such limitation and a number of specific developments have been described for the manufacture of structured surfaces at different scales [3]. Vibration assisted texturing, in particular, allows obtaining micro-dimples on the workpiece surface by oscillating the tool during the cutting process. This setup can be adapted to different machining strategies depending on the application, and has the potential to be cost-effective compared to other processes [4]. Ultrasonic Vibration-Assisted Machining (UVAM) has been investigated for improving the machinability of difficult-to-cut alloys, by lowering the cutting forces and tool wear as well as increasing the surface finish [5]. Additionally, UVAM, as a consequence of the superimposition of a high-frequency and small-amplitude vibration to the tool motion, makes it possible the generation of micro-textured surfaces with adequate geometrical accuracy, at reduced costs and processing times [6]. On the basis of the vibration pattern and parameters, cutting and tool characteristics, micro-dimples of different morphology and dimension can be obtained [7]. Furthermore, UVAM is versatile, as can be successfully applied to different kind of surfaces, e.g. flat and cylindrical [8]. In [9] UVAM was employed to generate hierarchical microstructures by means of overlapping elliptical tool trajectories, proving the attainment of a strong anisotropic wetting. Even if UVAM has been used for surface texturing, its ability to provide a surface capable to improve the adhesion of coatings has not been proved, yet.

In this context, the aim of the paper is to propose a novel machining-based surface texturing method, that is Cryogenic Ultrasonic Vibration-Assisted Turning (CUVAT), in which cryogenic cooling was applied for the first time to UVAM. This novel approach is intended to improve the performances of a sol-gel biocompatible coating on a magnesium alloy substrate in a human-like environment compared to that of conventionally fabricated surfaces. While UVAM allows the generation of a surface texture characterized by an enhanced wettability, cryogenic cooling increases the surface integrity [10], proving to have a synergistic effect on the coating performances.

The paper is divided into three parts: the first one is devoted to the description of the methods for the surface texture generation and related analyses to characterise the surface topography and integrity. The second part deals with the coating application and analysis of its performances in terms of coating thickness, adhesion strength and corrosion resistance. Finally, the third part presents the application case and the results of its functional testing after being corroded in a human-like environment.

2. Surface texture generation and characterization

For its attractiveness as bioresorbable metal, the investigated magnesium alloy was the AZ31, supplied in form of an annealed bar with average grain size of 15 µm.

The surface textures were generated using a Mori Seiki™ NL 2500 CNC lathe by means of 3 different turning operations: i) Conventional Turning (CT); ii) Ultrasonic Vibration-Assisted Turning (UVAT); iii) Cryogenic Ultrasonic Vibration-Assisted Turning (CUVAT).

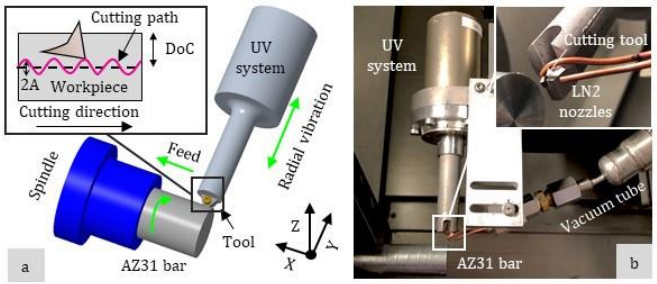

Figure 1. UVAT scheme (not to scale) (a), and CUVAT setup details (b).

The CNC lathe was equipped with an Ultrasonic Vibration (UV) system basically composed of three parts, namely a generator, a transducer, and a horn. More details about the UV system are given in [11]. Fig. 1a shows the UVAT setup with the reference system indicated. An apparatus comprising a Dewar, a vacuum jacketed hose, and two spray nozzles of diameter 0.9 mm, was combined to the UV system to deliver liquid nitrogen to the cutting zone. Fig. 1b shows the overall equipment for CUVAT with a zoom of the cryogenic cooling sub-system. A VCEX 110301L-F 1125 insert with rake angle (α) 5°30', clearance angle (β) 7°, and nose radius (R) 0.1 mm was used as cutting tool. During UVAT e CUVAT, the cutting tool vibrates in radial direction Y (see scheme in Fig. 1a) at a frequency (f_{us}) 30 kHz and amplitude (A) 5 µm. A preliminary UVAT campaign allowed choosing the cutting parameters that were afterwards kept constant: cutting speed (V) 100 m/min, feed (f) 0.05 mm/rev, and depth of cut (DoC) 0.05 mm. Since the depth of cut was significantly higher than the vibration amplitude, the tool never left the contact with the workpiece, making the cutting continuous as schematically shown in Fig. 1a. CT surfaces were generated as well as reference for sake of comparison. Both CT and UVAT were conducted under dry conditions. Three samples were generated for each machining strategy, and three different portions of the manufactured surfaces were characterized using the techniques described in the following.

Surface topography was evaluated using a Sensofar™ Plu-Neox optical profiler with a 20X magnification Nikon™ confocal objective. Areal surface texture parameters according to ISO 25178-2:2012 were computed after outliers and form removal using Gaussian filtering according to ISO 16610-61:2011 on the SL surface. Besides the average surface roughness (Sa) for general reference, the developed interfacial area ratio (Sdr), and the texture aspect ratio (Str) were considered as indicators of the generated surface wettability.

A Quanta 450 FEI™ Scanning Electron Microscope (SEM) allowed the scanning of the surface defects and evaluation of the Severe Plastic Deformed (SPD) layer below the machine surface as a consequence of the cutting process. Nanoindentations of the surface were performed using an iMicro™ by Nanomechanics Inc. nano-indenter equipped with a Berkovich diamond tip using a load of 25 mN, after polishing. The wettability of the generated surfaces was evaluated by means of a static sessile drop technique, using a distilled water droplet of 10 µm, whereas top view images of the droplets fallen on the surfaces were acquired through the optical profiler with a 10x Nikon™ confocal objective.

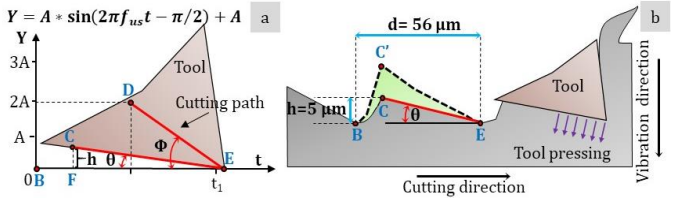

Figure 2. Theoretical cutting path at varying time (a), comparison between the theoretical and shifted profile of a dimple along the cutting direction (b).

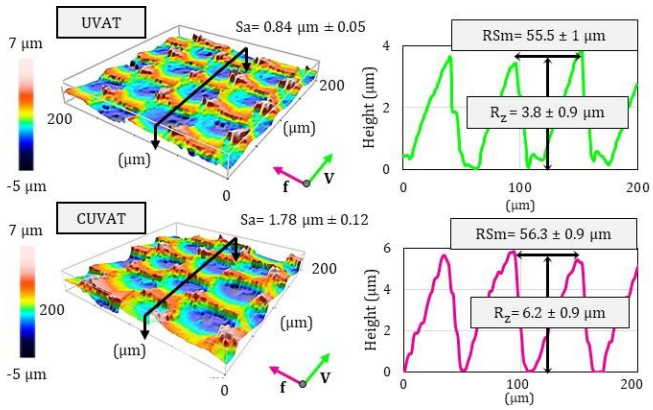

Figure 3. Textures of the UVAT and CUVAT surfaces.

The theoretical geometrical characteristics of the dimples were modelled on the basis of the cutting path represented by a sinusoid that is function of time (t), as shown in Fig. 2a [7].

The distance (d) between two adjacent dimples along the cutting direction, namely the dimples width, is given by Eq. (1):

$$d = V/f_{us} \qquad (1)$$

When the tool reaches point E (see Fig. 2a), its flank face intercepts the cutting path at point C, identifying an intersection angle (θ), which is approximately equal to the tool clearance angle (β). The intersection between the tool path and its flank face is identified through the intersecting ratio (σ) given by Eq. (2):

$$\sigma = \tan(\phi) = 4A/d \qquad (2)$$

Given the cutting conditions of the present study, the tool flank face always intercepts the cutting trajectory, being σ>tan(β). By considering triangle similarity criteria, the length of $\overline{CF}$ in Fig. 2a, namely the dimples depth (h), can be calculated through Eq. (3):

$$h = V * \frac{t_1}{1+tan\theta/tan\phi} * tan\beta \qquad (3)$$

where the time (t_1) is calculated as the ratio between d and V.

The mean width of the profile elements (RSm) and the maximum height of profile (Rz) computed on profiles extracted along the cutting direction were taken as indicators of the dimples width (d) and depth (h), respectively. Examples of textured surfaces from UVAT and CUVAT are shown in Fig. 3, which reports also the measured RSm and Rz values, whereas the values predicted on the basis of Eqs. (1) and (3) are reported in Fig. 2b. The experimental profiles show that dimples produced by CUVAT were significantly deeper than those by UVAT, which, instead, had depth closer to the theoretical one. As a matter of fact, the analytical modelling above reported does not take into account the effect of the elastoplastic deformation given by the cutting tool when it presses the material along the area CDE of Fig. 2a, which may induce changes in the profile compared to the theoretical one. The material indeed experiences elastic recovery after the tool disengagement, which is higher at the dimples' peaks, since the valleys are more plastically deformed by the tool pressing, therefore they recover less. As a consequence of the more pronounced elastic recovery at the peaks, the material shifts from point C to point C' (see Fig. 2b amplified). Nevertheless, this shift was higher in case of CUVAT due to the increased strain hardening induced by the lower temperatures of cryogenic cooling than those in case of UVAT. Therefore, due to that, CUVAT allowed the formation of deeper dimples than UVAT.

Table 1 Texture parameters of the generated surfaces.

	CT	UVAT	CUVAT
Sa (µm)	0.58 ± 0.02	0.84 ± 0.05	1.78 ± 0.12
Sdr (%)	0.72 ± 0.12	3.22 ± 0.11	16.5 ± 0.9
Str (%)	2.9 ± 0.1	14.3 ± 0.9	14.6 ± 0.7

Table 1 reports the texture parameters of the generated surfaces. Rougher surfaces in terms of Sa were generated by using UVAT and even more with CUVAT compared to CT. This is attributed to the presence of the dimples along the cutting direction. The hybrid parameter Sdr increased of 347% and 2192% when using UVAT and CUVAT compared to CT, respectively. The higher the Sdr the more complex the generated surface, and, furthermore, from the Wenzel theory, the higher the wettability thanks to the surface energy increase. The significant enhancement given by CUVAT is ascribed to the dimples' expansion along the vibration direction. The spatial parameter Str shows the more isotropic nature of the UVAT and CUVAT surfaces, as the dominant topography along the feed direction was mitigated by the one induced by the tool vibration in the radial direction. To more isotropic surfaces corresponds a more homogeneous spreading behaviour of the water droplets, and therefore enhanced wettability.

The surface energy, besides the texture, is driven by its metallurgical state: the higher the latter in terms of density of grain boundaries the more wettable the surface. In general, regardless of the approach for generating the surface, an SPD layer was always evident, with grains stretched and deformed along the cutting direction. The SPD layer extension set to comparable values for CT and UVAT, whereas it increased of 77% for CUVAT. Nanoindentations confirmed it, since a 21% increment of hardness was registered in the case of CUVAT (see Table 2).

In Fig. 4 the generated surfaces, Contact Angles (CA) and top views of the water droplets fallen on the surfaces are shown. Defects are hardly visible on the SEM images whatever the surface. The contact angles, measured perpendicular to the feed marks, proved a 17% and 30% wettability improvement of the UVAT and CUVAT surfaces compared to the CT one, respectively. Additionally, the top views of the water droplets show a more circular shape for those fallen on the UVAT and CUVAT surfaces, compared to the elliptical shape in the case of CT. Therefore, besides the wettability increase, the way ultrasonic vibrations were imposed reduced the anisotropic degree of wettability, as foreseen by the Str texture parameter.

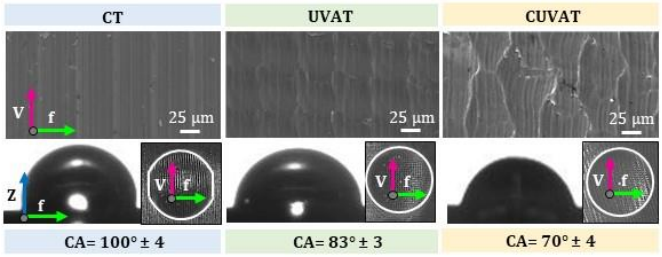

Figure 4. SEM images of the generated surfaces, contact angles and top views of the water droplets on the generated surfaces.

Table 2. Hardness (GPa) of the generated surfaces.

CT	UVAT	CUVAT
0.96 ± 0.04	1 ± 0.05	1.16 ± 0.05

3. Sol-gel coating application and characterization

A biocompatible sol-gel calcium phosphate (Ca-P)-based coating (see details of composition in [12]) was chosen to coat the generated surfaces because of its easiness in being applied, proven biocompatibility, and corrosion resistance to body fluids. In addition, calcium phosphate compounds belong to the orthophosphate group that is naturally present in several biological structures, including teeth and bones, which makes this coating more suitable for the specific application than other available [12]. However, sol-gel coatings show high sensitivity upon the substrate wettability. The fabricated samples were dip coated twice into the prepared solution and pulled off at the speed of 20 mm/min. Afterwards, they were dried at 80°C for 2 h and subsequently heated to 300°C for 1 hour. The coated samples were then cut, gold coated, embedded in epoxy resin, and polished to achieve a mirror-like surface. The coating thickness was measured from SEM images taken in multiple positions along both the feed and cutting speed directions. Fig. 5 shows the appearance of the generated surfaces after coating and reports also the coating average thickness. In general, all the coated surfaces appeared cracks-free. Nevertheless, the thickest coating was achieved on the CUVAT surface with a 253% increase compared to CT, whereas the increase was 141% in case of UVAT. Overall, the wettability increase given by the more complex and isotropic texture generated by UVAT and CUVAT favoured a more effective coating application. In fact, the more wettable the surface the lower the surface tension, which leads to thicker coatings according to the Landau-Levich equation. In addition, it is worth noting that the coating deposited within the dimples of the UVAT and CUVAT surfaces did not show any kind of delamination, whereas bubbles were present at the interface with the CT surface, as shown by the black dotted image in Fig. 5 of the CT surface after coating.

The coating adhesion, which is of primarily importance to provide a stable coating within the degradation period of the biomedical component, was evaluated by means of nanoindentations at the interface, indicated as one of the viable approaches in [13]. Due to the intrinsic variability of the measure, at least thirty indentations were performed on the polished samples. The load was fixed to 5 mN, low enough to guarantee the indentation at the coating interface. It is worth noting that the final heating after the coating application reduced the hardness of the bulk material to 0.82 ±0.01 GPa, regardless of the surface generation strategy, whereas the coating hardness settled to 0.37 ± 0.14 GPa. Table 3 reports the hardness of the coated interfaces: an increase of approximately 17% and 36% was found for UVAT and CUVAT surfaces compared to the CT one. The coating thickness is indeed a critical parameter that rules the shear strength of the interface [14]. The thicker the coating the stronger the adhesion, which explains the improvements provided by UVAT and CUVAT. Furthermore, the lower adhesion strength in case of the CT surface is also ascribed to the presence of the bubbles at the interface.

The corrosion behaviour of the coated and uncoated surfaces was assessed through Electrochemical Impedance Spectroscopy (EIS) tests by using a potentiostat (Amel™ 2549) coupled with a spectrometer (Materials Instrument™). The EIS tests were conducted in Simulated Body Fluid (SBF) solution at body temperature (37°C), at the value of the open circuit potential, using a frequency range between 10^5 and 10^{-2} Hz with a perturbation amplitude of 10 mV. Fig. 6a shows the equivalent circuit that was used to fit the EIS results, where Rs stands for the resistance of the solution, Rp for the polarization resistance, and CPE refers to a constant phase element.

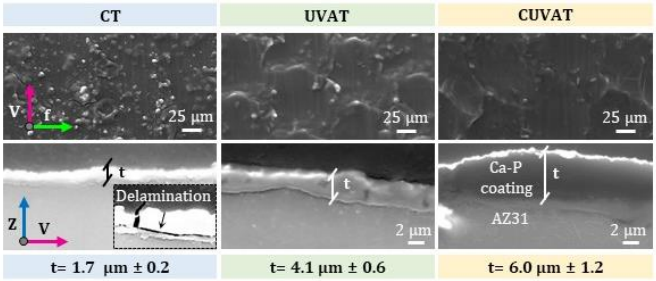

Figure 5. SEM images of the generated surfaces after coating and coating thickness.

Table 3. Hardness (GPa) of the coated interfaces.

CT	UVAT	CUVAT
0.53 ± 0.15	0.62 ± 0.18	0.72 ± 0.12

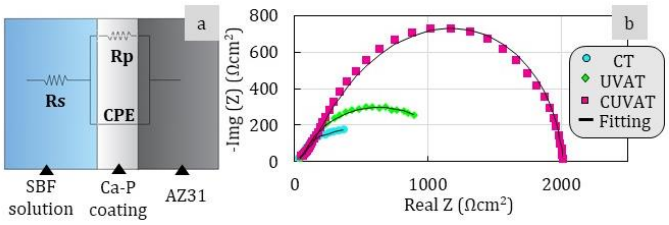

Figure 6. (a) Equivalent circuit of the EIS tests, and (b) experimental and fitted Nyquist plot of the coated samples (Z stands for impedance).

The portion of the circuit including the combination of Rp and CPE represents the interface between the electrolyte and the coating. The values of Rp are directly linked to the corrosion resistance offered by the coating, and are evaluated as the real part of the impedance (Z) at low frequencies in the Nyquist plot shown in Fig. 6b, where the points are the experimental data, and the continuous lines indicate the relative fitting. The Rp values calculated from the fitting using the equivalent circuit are given in Table 4. The uncoated surfaces generated through CT and UVAT settled to comparable values, whereas Rp increased of 36% for the CUVAT surface. The latter improvement is attributed to the increase of the SPD layer thickness and hardening. After coating, the Rp values noticeably increased thanks to the corrosion protection provided by the coating that played as an effective barrier against corrosive ions, regardless of the machining strategy. Rp increased of 92% for UVAT and 239% for CUVAT surfaces with respect to the CT one. Such improvements are ascribed to the coating thickness (Fig. 5) and bonding strength between the coating and the substrate (Table 3). Therefore, a synergistic effect of combining UVAT and cryogenic cooling is clearly seen, as the ultrasonic vibrations modify the texture and thus the wettability, further enhanced by cryogenic cooling that also improves the surface integrity.

Table 4. Rp (Ωcm^2) of the coated and uncoated surfaces.

	Uncoated surfaces	Coated surfaces
CT	50 ± 5	590 ± 10
UVAT	50 ± 4	1130 ± 15
CUVAT	68 ± 5	2000 ± 20

4. Application case

Pins used to fix small fragments of low solicited bones, like those of hands and feet, were considered as application case. These types of fractures completely heal after 3-6 weeks, after which the fixation pins are removed during cost- and pain-intensive secondary operations. Fixation pins made of bioresorbable metals must then assure their function of connecting the fractured bones for at least 3 weeks. Fig. 7a shows the rationale of such fixation pins. The pin chosen dimensions were 3.2 mm of diameter and 22 mm of length, the same of commercially available pins made either of stainless steels or titanium alloys. Standards indicating testing methods to qualify fixation pins are not available, nevertheless three points bending tests were carried out to evaluate their mechanical characteristics, following the ASTM F1541 standard for external skeletal fixation devices. Pins fabricated through CUVAT and then coated were tested before and after 3 weeks of immersion in SBF at body temperature, changing the solution every three days to avoid pH increase. For sake of comparison, also pins fabricated through CT were similarly tested, as CT represents the conventional fabrication method of fixation pins.

The three-point bending tests were performed using an Instron Electropuls E3000 (Norwood™, MA, US) equipped with a 5000 N load cell (Dynacell™ 2527-303) under displacement control (5 mm/min) and by adopting a span between supports equal to 14 mm: the obtained results are shown in Fig. 7b.

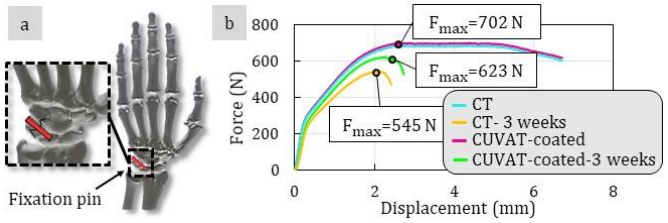

Figure 7. (a) Rationale of the fixation pin, and (b) bending force of the pins before and after being corroded.

The maximum bending load values of the CUVAT-coated and CT uncorroded pins were very similar and both did not break, proving that, prior to degradation, coating had no effect on the pin mechanical properties. In contrast, the load carrying capacity decreased by 11% and 22% compared to the initial value after 3 weeks for the CUVAT-coated and CT pins, respectively, confirming the lower degradation rate and more preservation of mechanical strength of the pin that was fabricated through the novel approach.

5. Conclusions

Ultrasonic vibration-assisted turning with cryogenic cooling was proved to generate a texture on AZ31 magnesium alloy substrate capable to enhance the performances of a biocompatible sol-gel coating in terms of increased corrosion resistance in a human-like environment compared to conventionally fabricated surfaces. In particular, modifications of the surface geometry and integrity, in form of deeper dimples, higher wettability and hardness, were understood as the major drivers to explain the increase of the coating performances. The proposed approach was successfully validated on pins used to fix low solicited bone fractures.

Acknowledgements

This research was carried out in the framework of the project PRIN 201742RB8R_002 "Bionic" funded by the Italian Ministry of University and Research.

References

[1] Bruschi S, Bertolini R, Ghiotti A, Savio E, Guo W, Shivpuri R (2018) Machining-induced surface transformations of magnesium alloys to enhance corrosion resistance in human-like environment. *CIRP Annals* 67(1):579-582.

[2] Ramsden JJ, Allen DM, Stephenson D, Alcock JR, Peggs GN, Fuller G, Goch G (2007) The design and manufacture of biomedical surfaces. *CIRP Annals* 56(2):687-711.

[3] Brinksmeier E, Karpuschewski B, Yan J, Schönemann L (2020) Manufacturing of multiscale structured surfaces. *CIRP Annals* 69(2):717–739.

[4] Bruzzone AAG, Costa HL, Lonardo PM, Lucca DA (2008) Advances in engineered surfaces for functional performance. *CIRP Annals* 57(2):750-769.

[5] M'Saoubi R, Axinte D, Soo SL, Nobel C, Attia H, Kappmeyer G, Engin S, Sim WM (2015) High performance cutting of advanced aerospace alloys and composite materials. *CIRP Annals* 64(2):557-580.

[6] Koyano T, Hosokawa A, Takahashi T, Ueda T (2019) One-process surface texturing of a large area by electrochemical machining with short voltage pulses. *CIRP Annals* 68(1):181-184.

[7] Liu X, Zhang J, Hu X, Wu D (2019) Influence of tool material and geometry on micro-textured surface in radial ultrasonic vibration-assisted turning. *International Journal of Mechanical Sciences* 152:545-557.

[8] Greco A, Raphaelson S, Ehmann K, Wang QJ, Lin C (2009) Surface texturing of tribological interfaces using the vibromechanical texturing method. *Journal of Manufacturing Science and Engineering* 131(6).

[9] Guo P, Lu Y, Ehmann KF, Cao J (2014) Generation of hierarchical micro-structures for anisotropic wetting by elliptical vibration cutting. *CIRP Annals* 63(1):553-556.

[10] Jawahir IS, Brinksmeier E, M'Saoubi R, Aspinwall DK, Outeiro JC, Meyer D, Umbrello D, Jayal AD (2011) Surface integrity in material removal processes: Recent advances. *CIRP Annals* 60(2):603-626.

[11] Di Iorio E, Bertolini R, Bruschi S, Ghiotti A (2018) Design and development of an ultrasonic vibration assisted turning system for machining bioabsorbable magnesium alloys. *Procedia CIRP* 77:324-327.

[12] Niu B, Shi P, Wei D, E S, Li Q, Chen Y (2016) Effects of sintering temperature on the corrosion behavior of AZ31 alloy with Ca–P sol–gel coating. *Journal of Alloys and Compounds* 665: 435-442.

[13] Duncan B, Crocker L (2001) Review of tests for adhesion strength. *National Physical Laboratory*.

[14] Zhang S, Wang YS, Zeng XT, Cheng K, Qian M, Sun DE, Weng WJ, Chia WY (2007) Evaluation of interfacial shear strength and residual stress of sol–gel derived fluoridated hydroxyapatite coatings on Ti6Al4V substrates. *Engineering Fracture Mechanics* 74(12):1884-1893.